

## Electronic Supplementary Information (ESI)

### Green synthesis of silver indium telluride nanocrystals: characterization and photothermal analysis

Felipe L. N. Sousa,<sup>a</sup> Brenand A. Souza,<sup>a</sup> Anderson J. Caires,<sup>b</sup> Severino A Júnior,<sup>a</sup> Denilson V. Freitas,<sup>a</sup> Marcelo Navarro<sup>a\*</sup>

<sup>a</sup>Departamento de Química Fundamental, Universidade Federal de Pernambuco, Cidade Universitária, 50670-901 Recife, PE, Brazil.

<sup>b</sup>Departamento de Engenharia Metalúrgica e Materiais, Universidade Federal de Minas Gerais, 31270-901 Belo Horizonte, MG, Brazil.

\*e-mail: marcelo.navarro@ufpe.br

#### Summary

1. Experimental	S2
2. $k_{sp}$ and solubility calculations for $In_2Te_3$ and $Ag_2Te$	S6
3. Supplemental results	S7
4. Time-resolved photoluminescence spectroscopy	S12
5. Photothermal performance	S14
6. Photothermal conversion efficiency ( $\eta_T$ )	S17
7. Comparison among synthetic methodologies	S18
8. References	S20

## 1. Experimental

### 1.1. Materials

Silver(I) nitrate ( $\text{AgNO}_3$  anhydrous, 99.99%), indium(III) nitrate hydrate ( $\text{In}(\text{NO}_3)_3 \cdot x\text{H}_2\text{O}$ , 99.99%), sodium perchlorate ( $\text{NaClO}_4$ ,  $\geq 98\%$ ), elemental tellurium powder ( $\text{Te}^0$ , 99.99%, -100 mesh), elemental selenium powder ( $\text{Se}^0$ , 99.99%, -100 mesh), elemental sulfur powder ( $\text{S}^0$ , 99.98%, -100 mesh), L-glutathione (GSH,  $\geq 98\%$ ), citric acid (CA,  $\geq 98\%$ ) and graphite powder (particle size  $< 20 \mu\text{m}$ ) were purchased from Sigma-Aldrich. The elemental zinc (Zn, 99.9%) bar was purchased from Goodfellow. Ethanol and acetone were of P.A. grade and purchased from Dynamic. All reagents were used without prior purification. Aqueous solutions were prepared with deionized Milli-Q water ( $17.0 \Omega \cdot \text{cm}^{-1}$ ). Stock solutions of  $\text{AgNO}_3$  ( $0.25 \text{ mol} \cdot \text{L}^{-1}$ ) and  $\text{In}(\text{NO}_3)_3 \cdot x\text{H}_2\text{O}$  ( $0.25 \text{ mol} \cdot \text{L}^{-1}$ ) were prepared in water and ethanol, respectively.

### 1.2. Electrosynthesis of $\text{AgIn}_5\text{Te}_8/\text{GSH}$ (AITe)

The tellurium electroreduction methodology was previously described and applied with some modifications.<sup>1,2</sup> An electrochemical cavity cell was used, the cathodic compartment of the electrochemical cavity cell (graphite powder macroelectrode) was filled with graphite powder (6.0 mmol) and elemental tellurium (0.0050, 0.0125, 0.0250, 0.0375, or 0.050 mmol), and the mixture was pressed under  $P = 3.2 \text{ kg} \cdot \text{cm}^{-2}$  for 10 min. A sintered glass (1.0 cm diameter) was sonicated in  $0.1 \text{ mol} \cdot \text{L}^{-1}$   $\text{NaClO}_4$  aqueous solution, and then placed over the cavity to avoid the dispersion of the graphite. This procedure allows the decrease in the liquid junction potential and migration of  $\text{Te}^{2-}$  ions formed during the electroreduction. A stainless-steel grid was used as an anode, placed into the anodic compartment containing  $1.0 \text{ mol} \cdot \text{L}^{-1}$   $\text{NaOH}$  solution, and separated from the intermediate compartment by a Nafion<sup>®</sup> membrane.

The ternary  $\text{AgIn}_5\text{Te}_8/\text{GSH}$  nanocrystals were prepared by controlling the  $\text{Ag}^+/\text{In}^{3+}$  ratio in solution.  $0.25 \text{ mol} \cdot \text{L}^{-1}$   $\text{AgNO}_3$  aqueous solution ( $\text{Ag}^+_{\text{Volume}} = 133 \mu\text{L}$ ) and  $0.25 \text{ mol} \cdot \text{L}^{-1}$   $\text{In}(\text{NO}_3)_3$  ethanoic solution ( $\text{In}^{3+}_{\text{Volume}} = 66.5 \mu\text{L}$ ) were used to prepare  $\text{Ag}^+/\text{In}^{3+}$  precursor solution (2:1) in 10 mL of MilliQ water. 0.25 mmol L-glutathione

(GSH) + 0.25 mmol citric acid (CA) stabilizers were dissolved in 10 mL of MilliQ water and added to the  $\text{Ag}^+/\text{In}^{3+}$  solution, followed by 5 mL of  $0.5 \text{ mol.L}^{-1}$   $\text{NaClO}_4$  solution, and the pH was corrected to pH 8 by dropwise of  $1.0 \text{ mol.L}^{-1}$   $\text{NaOH}$  solution. Electrolyses to get AlTe were carried out according the initial number of moles of  $\text{Te}^0 = 0.005, 0.0050, 0.0125, 0.0250, 0.0375,$  or  $0.050$  mmol. The theoretical charges were calculated according to  $Q_T = n \times 2e^- \times 96,487 \text{ C.mol}^{-1}$ . Thus, the respective  $Q_T$  where  $0.96, 2.14, 4.82, 7.24,$  and  $9.64$  C, respectively. To ensure the complete electroreduction of  $\text{Te}^0$  (*i.e.*, 100% conversion  $\text{Te}^0 \rightarrow \text{Te}^{2-}$ ), it was passed an additional 20% charge. According to equation  $Q = i \times t$ , the electrolysis times where  $t = 1.2 \times Q_T / i = 0.03$  A, or  $t = 39, 86, 193, 290,$  and  $386$  s, respectively. The  $\text{AgIn}_5\text{Te}_8$  seeds were heated ( $100 \text{ }^\circ\text{C}$ ) for 1, 2, 3, 4, 5, 10, 20 and 30 min, and stored at  $4 \text{ }^\circ\text{C}$ .

### 1.3. Electrosynthesis of ZnS/GSH and ZnSe/GSH seeds

The ZnS and ZnSe seeds stock solutions were prepared by using the procedure described by Silva (2021).<sup>3</sup> The electrosyntheses were carried out by the paired electrolysis method, where a bar of zinc was used as sacrificial anodic and  $\text{Zn}^{2+}$  ion precursor.  $\text{S}^{2-}$  or  $\text{Se}^{2-}$  ions were generated in the cathodic cavity from the reduction of elemental sulfur or selenium, in the graphite powder macroelectrode.<sup>3</sup> The cavity cell macroelectrode was prepared by mixing 38.3 mg (3.2 mmol) of graphite powder and 0.25 mmol of the chalcogenide precursor (8.1 mg of  $\text{S}^0$  or 19.7 mg of  $\text{Se}^0$ ). Graphite and chalcogenide powders were added to the cathodic cavity and pressed ( $P = 3.2 \text{ kg.cm}^{-2}$ ) during 10 min. A sintered glass (1.0 cm diameter) was sonicated in  $0.1 \text{ mol.L}^{-1}$   $\text{NaClO}_4$  aqueous solution and then placed over the cavity. 153.7 mg (0.51 mmol) of GSH and 150.0 mg (2.6 mmol) of  $\text{NaClO}_4$  were dissolved in 25 mL of deionized water, and the pH adjusted to 7 by dropwise addition of  $1.0 \text{ mol.L}^{-1}$   $\text{NaOH}$  solution and added to the central compartment of the cavity cell.  $\text{Zn}^0$  bar was used as sacrificial anode. A paired electrolysis was carried out at 30 mA constant current during 1,608 s ( $Q = 48$  C), under argon. The pH of the  $\text{ZnX-GSH}$  (X: S or Se) seeds solution was adjusted to 9 and stored (without heating treatment) at  $4 \text{ }^\circ\text{C}$ , under dark conditions.

#### 1.4. Preparation of AgIn<sub>5</sub>Te<sub>8</sub>/ZnX (X = S, Se) nanocrystals

AgIn<sub>5</sub>Te<sub>8</sub>/ZnX nanocrystals (X = S, Se) were chemically prepared by mixing the ZnX seeds and the AgIn<sub>5</sub>Te<sub>8</sub> NCs solutions (core NCs Ag<sup>+</sup>/In<sup>3+</sup>: 2:1, heated by 5 min). The AgIn<sub>5</sub>Te<sub>8</sub>/ZnX ratio was determined by considering the equivalent number of the respective chalcogenide ions, X<sup>2-</sup>/Te<sup>2-</sup> given ratios: 0.25, 0.50, 1.00, and 1.50, followed by heating at 100 °C, for 5 min. This step was realized to determine the ideal conditions to promote the shift of the emission band to visible region. In both cases, the concentrations of the AgIn<sub>5</sub>Te<sub>8</sub>/ZnS and AgIn<sub>5</sub>Te<sub>8</sub>/ZnSe NCs were determined assuming an electrochemical yield of 100%. Then, the final solutions were stored at 4 °C and dark conditions.

#### 1.5. Absorption and Emission Spectra

Absorption spectra were carried out in quartz cuvettes using an Agilent 8453 UV-Vis spectrophotometer. Tauc curves were used to determine the optical E<sub>g</sub>. The emission spectra of AgIn<sub>5</sub>Te<sub>8</sub> colloidal nanoparticles were registered using a Duetta Horiba spectrofluorometer (with excitation slit 5 mm and emission slit 10 mm). The emission spectra were obtained using a Fluorolog-3 Horiba Jobin Yvon spectrofluorometer (with excitation and emission slit 3 mm) at λ<sub>exc</sub> = 488 nm. Photoluminescence decay (PL decay) curves of all the NCs were carried out at λ<sub>exc</sub> = 339 nm (Nanoled - Horiba), observing the maximum emission for each sample. The photoluminescence QY was determined at room temperature by comparing the integrated emission intensity of AlTe, AlTe/ZnS and AlTe/ZnSe NCs in solution, and compared to the rhodamine 6G (R6G) standard in anhydrous ethanol, QY = 95% at identical optical density, λ<sub>exc</sub> = 488 nm.<sup>4</sup>

#### 1.6. Structural and Morphological Investigation

The crystalline structure of the nanocrystals was obtained using powder X-ray diffraction (PXRD) (D8 Advance - Rigaku) equipped with an X-ray tube (Cu K<sub>α</sub>: 1.5418 Å, 40 kV, 40 mA, 2θ range from 10° to 80°, in steps of 0.02°). The nanocrystals were

precipitated using a 1:1 ratio of acetone/colloidal solution, subjected to centrifugation (30 min, 6000 rpm) and washed with ethanol. The samples were dried under vacuum, macerated in an agate mortar, and the powder was stored under a dry atmosphere.

The morphological and structural characterization of the AlTe NCs, and AlTe/ZnS and AlTe/ZnSe alloys NCs were based on high-resolution transmission electron microscope HRTEM images, energy dispersive X-ray spectrometry (EDS). A JEOL JEM-2100Plus HRTEM was used (JEOL<sup>®</sup>, Japan), with 200 kV acceleration potential, with nickel-coated carbon screens (Electron Microscopy Sciences, USA) as the support for the nanoparticles, followed by complete drying at low pressure overnight. The size distribution of the nanoparticles was obtained based on HRTEM images, randomly selecting 200 nanoparticles, using the image processing program (ImageJ, version 1.50, public domain, National Institutes of Health).

### 1.7. Photothermal Response and Measurements

To evaluate the photothermic performance of the AlTe, AlTe/ZnS and AlTe/ZnSe NCs, as powders and as colloids, the Ocean Optics near-infrared laser ( $\lambda_{exc} = 785 \text{ nm}$ ) was used, with optical fiber, fiber core size 1000  $\mu\text{m}$ . The photothermal response measurements of the NC powders (5 mg in porcelain spot plate), a FLIR E5 infrared camera was positioned at 10 cm of the sample (tilt 45°), and the distance between the probe and sample was 5 cm. The solid samples were irradiated during 1 min, and the power density was varied between 400  $\text{mW}\cdot\text{cm}^{-2}$  and 1.000  $\text{mW}\cdot\text{cm}^{-2}$ . The uncovered porcelain spot plate was used as a negative control. To colloidal nanoparticles photoresponse, all samples were patterned by the absorption band (0.2) at  $\lambda_{exc} = 785 \text{ nm}$ . 250  $\mu\text{L}$  of the colloid solutions were disposed in Eppendorf tubes, and the distance between the probe and sample was 5 cm. The FLIR E5 camera was positioned at 10 cm of sample (tilt 90°). They were registered 5 cycles on-off. The colloidal samples were irradiated during 10 min, and the power density was varied between 400  $\text{mW}\cdot\text{cm}^{-2}$  and 1.000  $\text{mW}\cdot\text{cm}^{-2}$ . The same distilled water volume was used as a negative control.

Colloid stability was determined by irradiation of 1 mL of AlTe, AlTe-ZnS and AlTe-ZnSe colloidal solutions under identical conditions for the measurement of the photothermal cycles, and continuously irradiated for 30 min with a laser powder of 1.0 W.cm<sup>-2</sup>, and the absorption spectra were recorded. The surface charge value of the nanocrystals was measured before and after irradiation, via zeta potential (ZP) measurements. Using ZetaPlus equipment (Brookhaven Instruments Corporation, 35 mW red laser light, wavelength  $\lambda = 660$  nm from 25 points. ZP measurements were carried out at  $25 \pm 2$  °C using the Smoluchowski approximation method in a set of 25 replicates.

## 2. $k_{sp}$ and solubility calculations for $In_2Te_3$ and $Ag_2Te$

The  $k_{sp}$  ( $In_2Te_3$ ) value was estimated from Gibbs free energy and  $K_{sp}$  equations:

$$\Delta G_f^\circ = \Delta H_f^\circ - TS_f^\circ$$

$$\Delta G_f^\circ = -RT \cdot \log(k_{sp})$$

where,  $\Delta H_f^\circ = -191.627$  kJ.mol<sup>-1</sup>,  $S_f^\circ = 234.304$  J.mol<sup>-1</sup>.K<sup>-1</sup>,  $T = 298$  K, and  $R = 8.31$  J.mol<sup>-1</sup>.K<sup>-1</sup>.<sup>5</sup>

$$k_{sp} (In_2Te_3) = 1 \times 10^{-106}$$

The same  $k_{sp}$  estimation was carried out for  $Ag_2Te$ , where,  $\Delta H_f^\circ = -35.982$  kJ.mol<sup>-1</sup>,  $S_f^\circ = 153.553$  J.mol<sup>-1</sup>.K<sup>-1</sup>,  $T = 298$  K, and  $R = 8.31$  J.mol<sup>-1</sup>.K<sup>-1</sup>.<sup>5</sup>

$$k_{sp} (Ag_2Te) = 1 \times 10^{-66}$$

### *Solubility calculation for $In_2Te_3$ and $Ag_2Te$*

In order to compare the solubility of  $In_2Te_3$  and  $Ag_2Te$ , the metal valences must be taken into account based on the corresponding dissociation reactions:



According to these reactions, the solubility products can be written as:

$$K_{SP}(\text{In}_2\text{Te}_3) = [\text{In}^{3+}]^2 \times [\text{Te}^{2-}]^3 = [\text{In}^{3+}]^2 \times [3/2 \times \text{In}^{3+}]^3 = 1 \times 10^{-106}, \text{ and}$$

$$K_{SP} \text{Ag}_2\text{Te} = [\text{Ag}^+]^2 \times [\text{Te}^{2-}] = [\text{Ag}^+]^2 \times [1/2 \text{Ag}^+] = 1 \times 10^{-66}$$

thus, one has to compare:

$$[\text{In}^{3+}] = \sqrt[5]{8/27 K_{SP} \text{In}_2\text{Te}_3} = 5.0 \times 10^{-22} \text{ with } [\text{Ag}^+] = \sqrt[3]{2 K_{SP} \text{Ag}_2\text{Te}} = 1.7 \times 10^{-22}.$$

### 3. Supplemental results

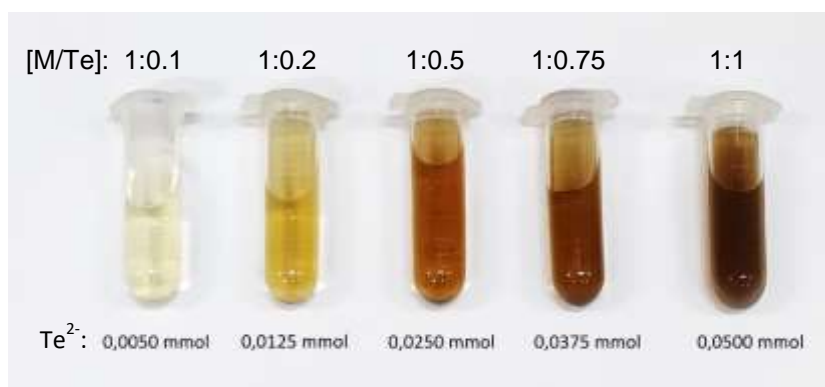


**Figure S1.** AlTe samples prepared at different  $M/\text{Te}^{2-}$  ( $M = \text{Ag}^+ + \text{In}^{3+}$ ) ratios (1:0.1, 1:0.2, 1:0.5, 1:0.75 and 1:1) co-stabilized by GSH and CA. Solutions were heated for 5 min at 100 °C under ambient light. ( $M = 1.33 \text{ mmol.L}^{-1} \text{Ag}^+ + 0.664 \text{ mmol.L}^{-1} \text{In}^{3+}$ ).

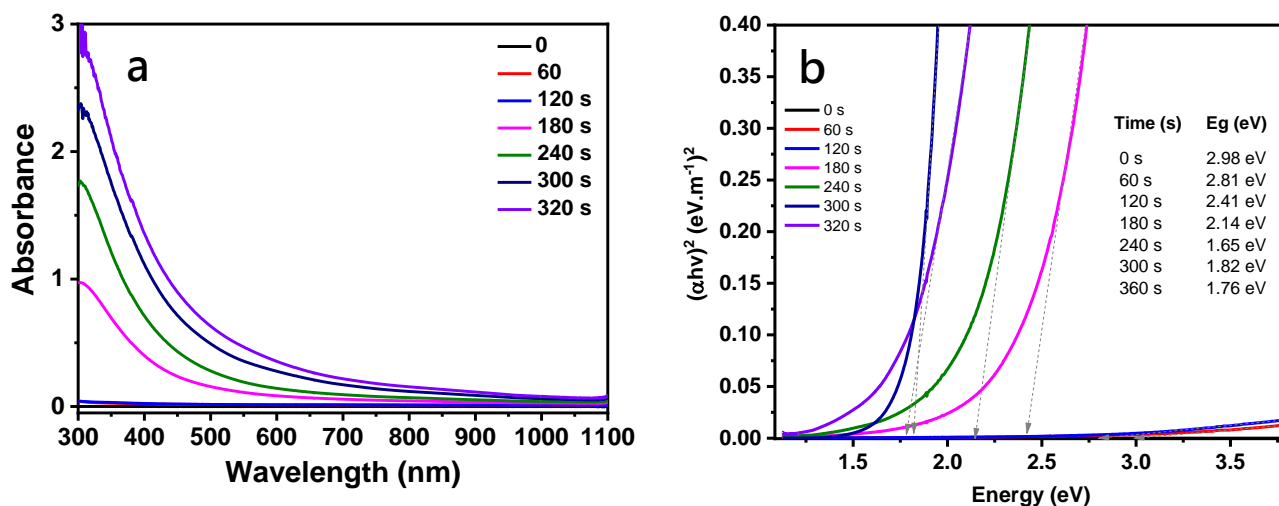


**Figure S2.** (a) UV-Vis-NIR absorption spectra taken during AlTe electrosynthesis ( $M/\text{Te}^{2-}$  ratio = 1:0.75, co-stabilized by GSH and CA, where  $M = 1.33 \text{ mmol.L}^{-1} \text{Ag}^+ + 0.664 \text{ mmol.L}^{-1} \text{In}^{3+}$ ). Spectra were taken at  $t = 0, 60, 120, 180, 240, 300$  and  $320$  s. (b) Tauc plots were obtained from AlTe absorption spectra during electrolysis time.

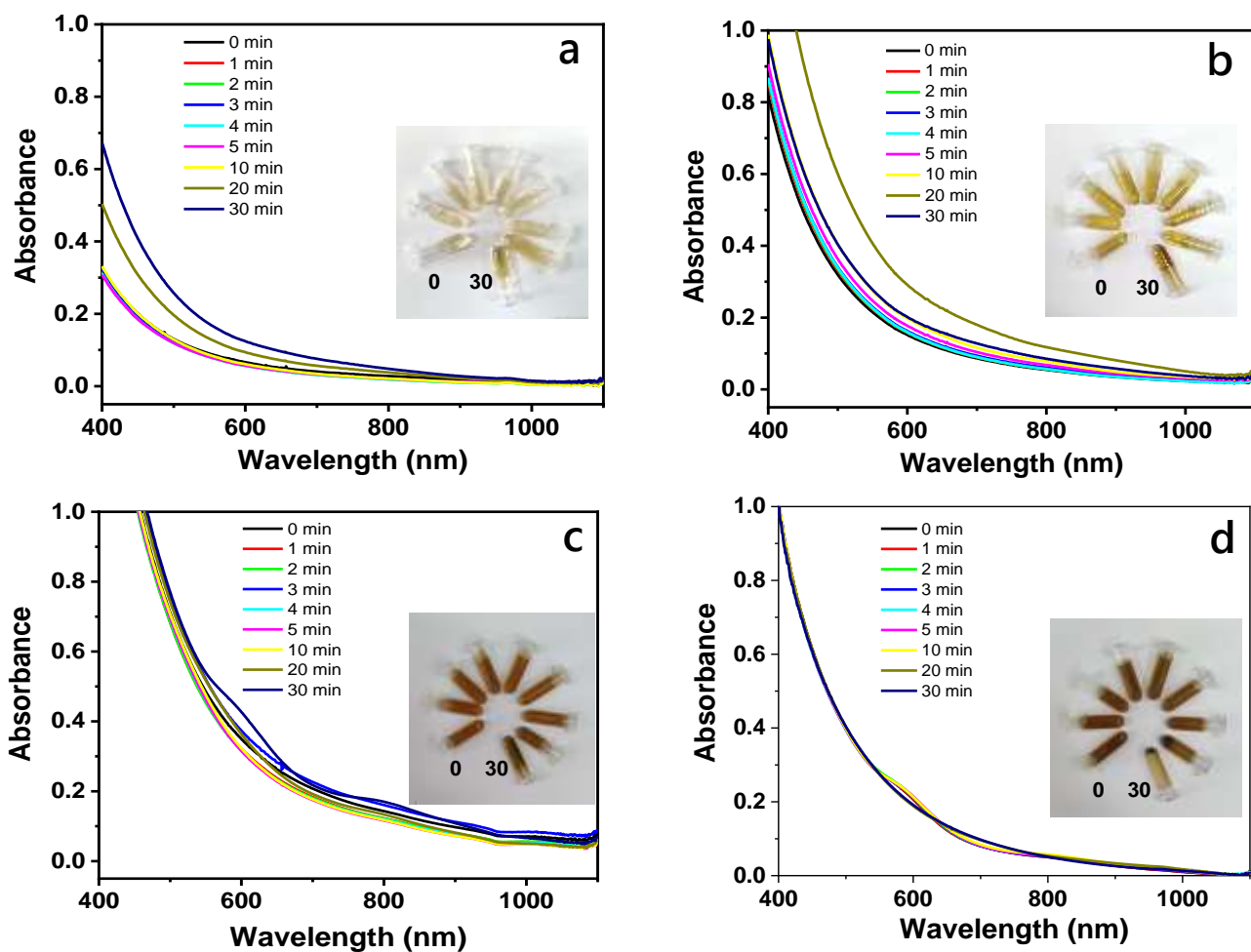


**Figure S3.** UV-Vis-NIR absorption spectra of AlTe samples prepared at different M/Te<sup>2-</sup> ratios: (a) 1:0.1, (b) 1:0.2, (c) 1:0.5, and (d) 1:0.75. All reactions were carried out by using GSH and CA as stabilizers. All samples were heated at 100 °C for 1, 2, 3, 4, 5, 10, 20, and 30 min, and ambient light. Ag<sup>+</sup>/In<sup>3+</sup> concentration = 1.33 mmol.L<sup>-1</sup> Ag<sup>+</sup> + 0.664 mmol.L<sup>-1</sup> In<sup>3+</sup>. All spectra were registered 5 minutes after the heating process, and inset photographs were registered 20 minutes after the heating process.

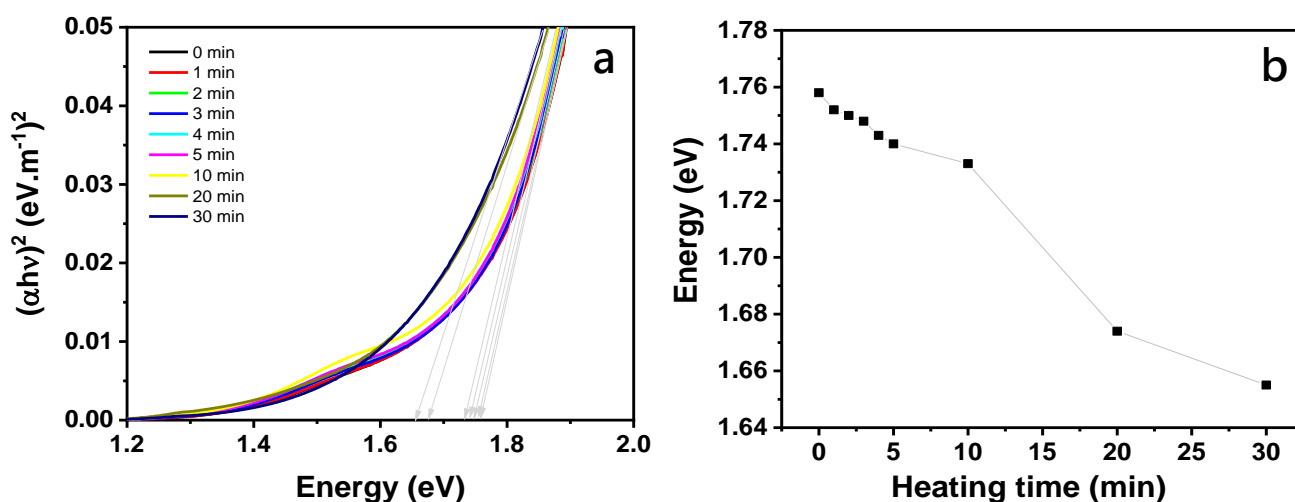


**Figure S4.** Thermal treatment step for AlTe NCs. (a) Tauc plots obtained from absorption spectra of AlTe NCs solution (M/Te<sup>2-</sup> ratio = 1:0.75, co-stabilized by GSH and CA, where M = 1.33 mmol.L<sup>-1</sup> Ag<sup>+</sup> + 0.664 mmol.L<sup>-1</sup> In<sup>3+</sup>). Heating time = 0, 1, 2, 3, 4, 5, 10, 20 and 30 min. (b) Eg vs. heating time.

**Table S1.** Ionic radii of the elements used to prepare the AlTe, AlTe/ZnS and AlTe/ZnSe NCs: Ag<sup>+</sup>, In<sup>3+</sup>, Te<sup>2-</sup>, Zn<sup>2+</sup>, S<sup>2-</sup>, and Se<sup>2-</sup>.\*

Entry	Ion	Ionic radii (Å)
1	Ag <sup>+</sup>	1.15
2	In <sup>3+</sup>	0.8
3	Te <sup>2-</sup>	2.21
4	Zn <sup>2+</sup>	0.74
5	S <sup>2-</sup>	1.84
6	Se <sup>2-</sup>	1.98

\*R.D. Shannon, "Revised Effective Ionic Radii and Systematic Studies of Interatomic Distances in Halides and Chalcogenides", Acta Cryst. A32 751-767 (1976).

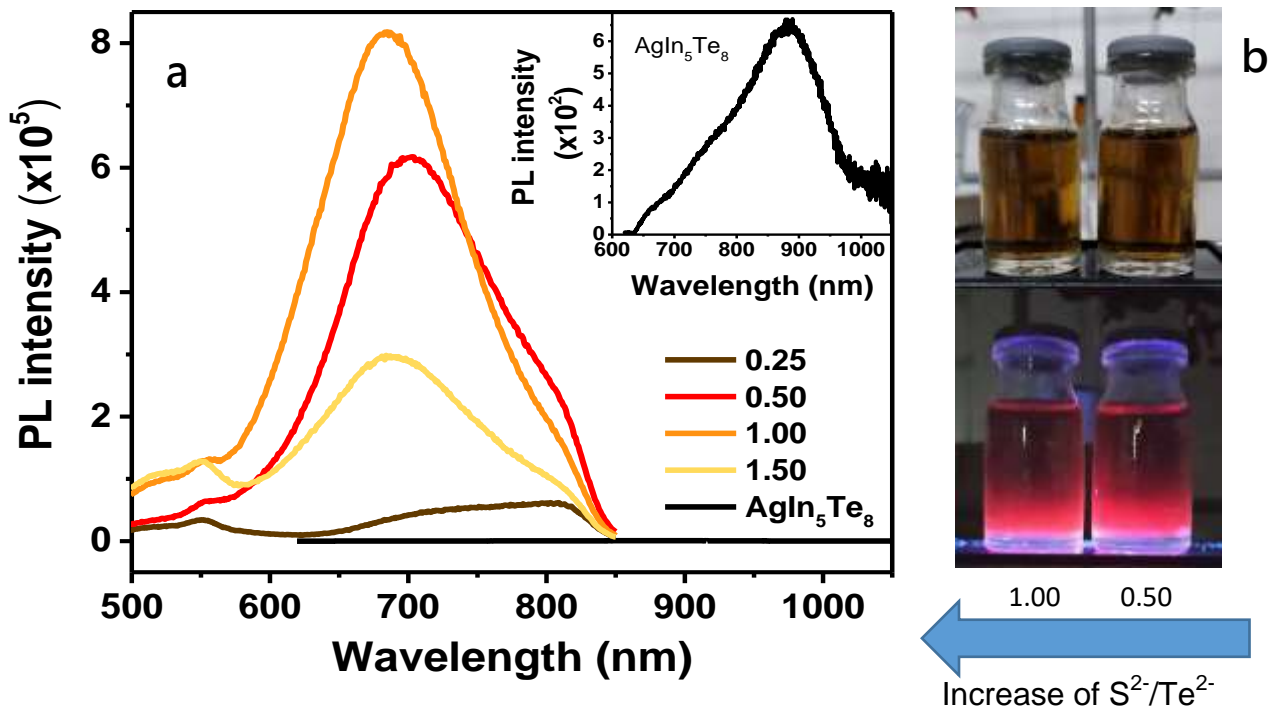
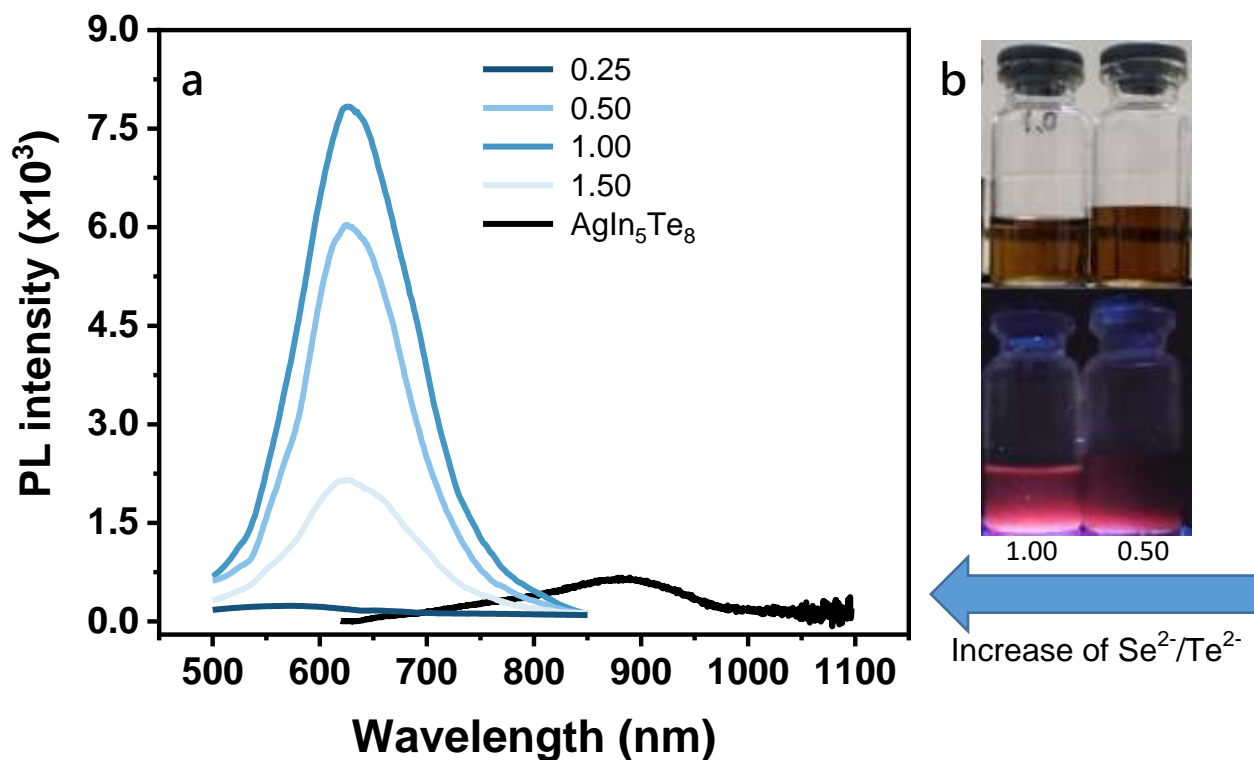


Figure S5. Photoluminescence intensity of AgIn<sub>5</sub>Te<sub>8</sub> and AgIn<sub>5</sub>Te<sub>8</sub>/ZnS according to S<sup>2-</sup>/Te<sup>2-</sup> ratio = 0.25, 0.50, 1.00, and 1.50 (M/Te<sup>2-</sup> ratio = 1:0.75), co-stabilized by GSH and CA, where M = 1.33 mmol.L<sup>-1</sup> Ag<sup>+</sup> + 0.664 mmol.L<sup>-1</sup> In<sup>3+</sup>. Heating time = 5 min. Inset of AgIn<sub>5</sub>Te<sub>8</sub> spectrum was magnified to PL intensity x10<sup>2</sup> for better visualization. (b) AgIn<sub>5</sub>Te<sub>8</sub>/ZnS colloidal solutions.



**Figure S6.** (a) Photoluminescence intensity of  $\text{AgIn}_5\text{Te}_8$  and  $\text{AgIn}_5\text{Te}_8/\text{ZnSe}$  according to  $\text{Se}^{2-}/\text{Te}^{2-}$  ratio = 0.25, 0.50, 1.00, 1.50.  $\text{M}/\text{Te}^{2-}$  ratio = 1:0.75, co-stabilized by GSH and CA, where  $\text{M} = 1.33 \text{ mmol.L}^{-1} \text{Ag}^+ + 0.664 \text{ mmol.L}^{-1} \text{In}^{3+}$ ). Heating time = 5 min. (b)  $\text{AgIn}_5\text{Te}_8/\text{ZnSe}$  colloidal solutions.

**Table S2.** Optical properties of  $\text{AlTe}$  ( $\text{M}/\text{Te}^{2-} = 1:0.75$ ) and  $\text{AlTe-ZnX}$  ( $\text{X} = \text{S}, \text{Se}$ ) systems:  $E_g$ , maximum wavelength emission ( $\lambda_{em}$ ), full width at half maximum (FWHM), and quantum yield (QY) using Rhodamine R6G standard.

Entry	Sample*	$E_g$ (eV)	$\lambda_{em}$ (nm)	FWHM (nm)	QY (%)
1	AlTe	1.60	889	319	-
2	$\text{S}^{2-}/\text{Te}^{2-} = 0.50$	1.77	703	112	0.27
3	$\text{S}^{2-}/\text{Te}^{2-} = 1.00$	1.75	685	126	0.34
4	$\text{Se}^{2-}/\text{Te}^{2-} = 0.50$	1.80	625	145	0.01
5	$\text{Se}^{2-}/\text{Te}^{2-} = 1.00$	1.80	625	133	0.04

\*The photothermic applications were selected for the samples with the most intense PL, the alloys with  $\text{X}^{2-}/\text{Te}^{2-}$  ratio = 0.50 and 1.00.

#### 4. Time-resolved photoluminescence spectroscopy

Fig. S7 shows the photoluminescence decay (PL decay) curves of all the QDs at an excitation of 339 nm (Nanoled - Horiba). The PL decay was recorded at 890 nm, 685 nm, and 632 nm for AlTe core, AlTe-ZnS ( $S^{2-}/Te^{2-} = 0.50$  and 1.00), and AlTe-ZnSe ( $Se^{2-}/Te^{2-} = 0.50$  and 1.00), respectively. The PL decay curves for core/shell QDs were fitted to a three-exponential equation (1):

$$I(t) = A_1 \exp\left(-\frac{t}{\tau_1}\right) + A_2 \exp\left(-\frac{t}{\tau_2}\right) + A_3 \exp\left(-\frac{t}{\tau_3}\right) \quad (1)$$

where,  $I(t)$  is the PL intensity resolved in time  $t$ ;  $A_1$ ,  $A_2$  and  $A_3$  are the relative amplitudes; and  $\tau_n$  are lifetimes. Each one is correlated to a specific process of electron recombination: the shortest  $\tau_1$  is related to the excitonic process, while long lifetimes,  $\tau_2$  and  $\tau_3$ , are corresponded at electronic transitions involving surface defects such incomplete bonds ( $\tau_2$ ), and donor-acceptor states ( $\tau_3$ ).<sup>6-8</sup> For average lifetime were used the equation  $\tau_{avg} = (A_1\tau_1^2 + A_2\tau_2^2 + A_3\tau_3^2)/(A_1\tau_1 + A_2\tau_2 + A_3\tau_3)$ . For AlTe core the fit of experimental curve followed a double exponential equation. The results are presented in Table S3.

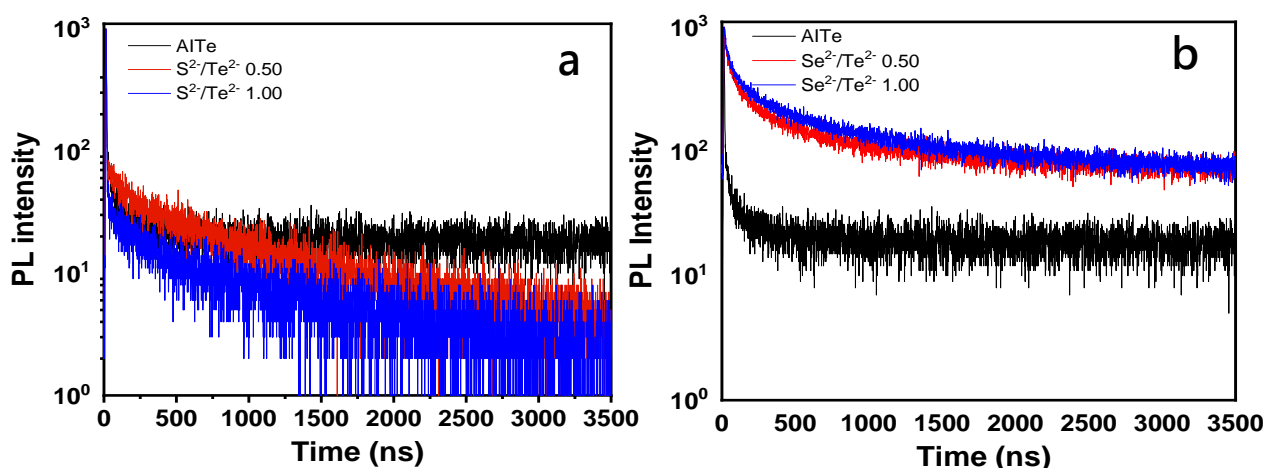


**Figure S7.** Photoluminescence decay curves for AlTe and AlTe-ZnX (X = S, Se) NCs at different  $S^{2-}/Te^{2-}$  and  $Se^{2-}/Te^{2-}$  ratios (0.50 and 1.00).  $M/Te = 1:0.75$ ,  $M = 1.33 \text{ mmol.L}^{-1} \text{ Ag}^+ + 0.664 \text{ mmol.L}^{-1} \text{ In}^{3+}$ .

**Table S3.** Time-resolved emission data: amplitudes ( $A_1$  and  $A_2$ ), time constants ( $\tau_1$  and  $\tau_2$ ) and average lifetime ( $\tau_{avg}$ ) for AlTe and AlTe-ZnX (X = S, Se) NCs.

Entry	Sample	$\tau_1$ (ns)	$A_1$	$\tau_2$ (ns)	$A_2$	$\tau_3$ (ns)	$A_3$	$\tau_{ave}$ (ns)
1	AlTe	0.022	99.96	21.54	0.04	-	-	6.08
2	AlTe-ZnS 0.50	0.025	98.98	24.83	0.1	217.27	0.91	212.26
3	AlTe-ZnS 1.00	0.021	99.93	27.35	0.01	198.37	0.07	169.89
4	AlTe-ZnSe 0.50	2.90	5.72	25.64	24.13	172.02	70.15	164.66
5	AlTe-ZnSe 1.00	2.94	4.39	30.03	18.81	205.12	76.81	198.90

For the AlTe the were registred that only excitonic and surface traps contribution for NIR luminescence, obtaining a total average lifetime of 6.08 ns. With the introduction of ZnS and ZnSe were observed the increase in the contribution of surface traps ( $\tau_2$ ) and an arising of donor-acceptor recombination ( $\tau_3$ ), followed by an increase of  $\tau_{avg}$ . Two concurrent effects are related to this behaviour: the epitaxial growth of the shell and an alloying process mediated by ion exchange.<sup>9,10</sup>

## 5. Photothermal performance

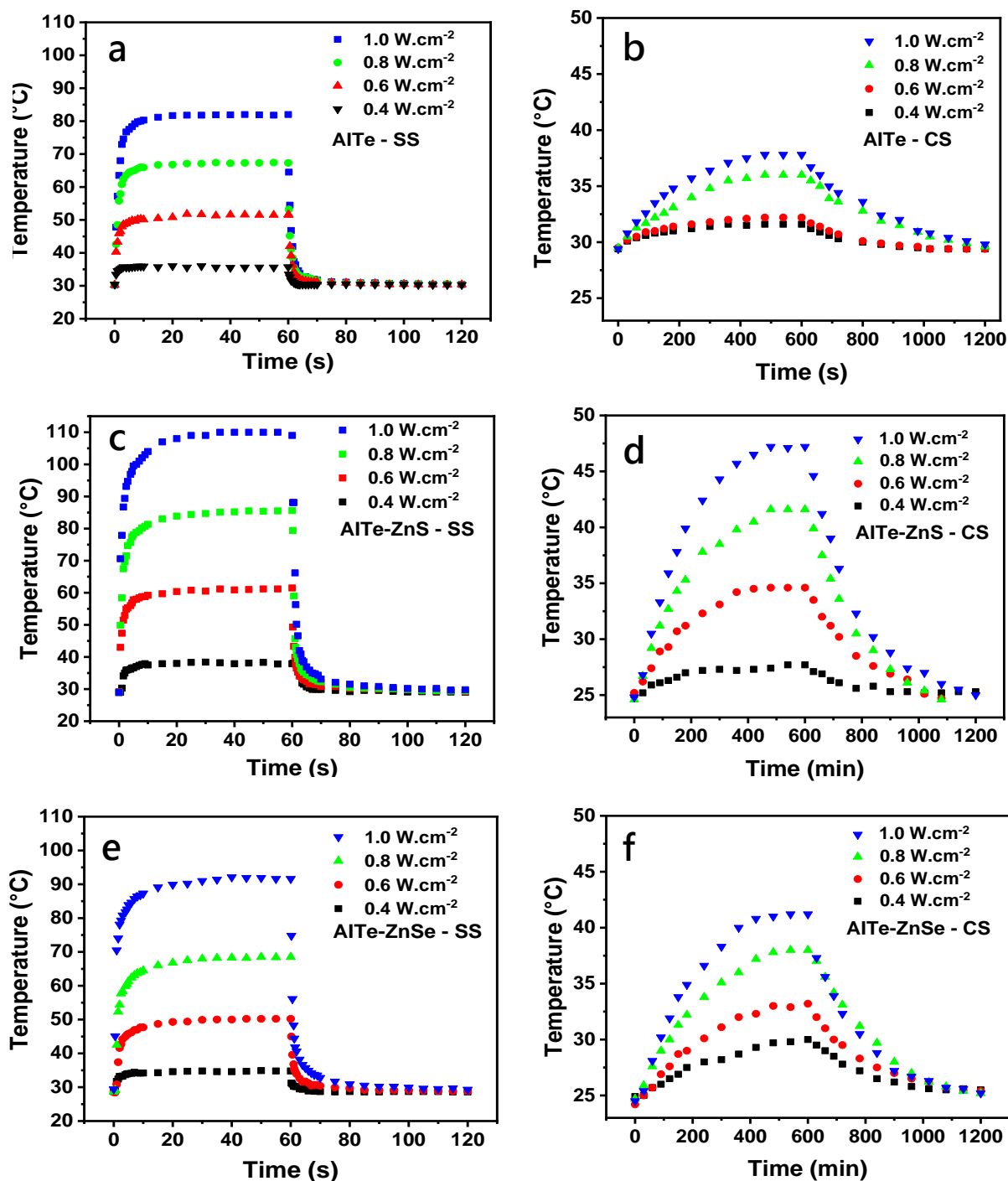
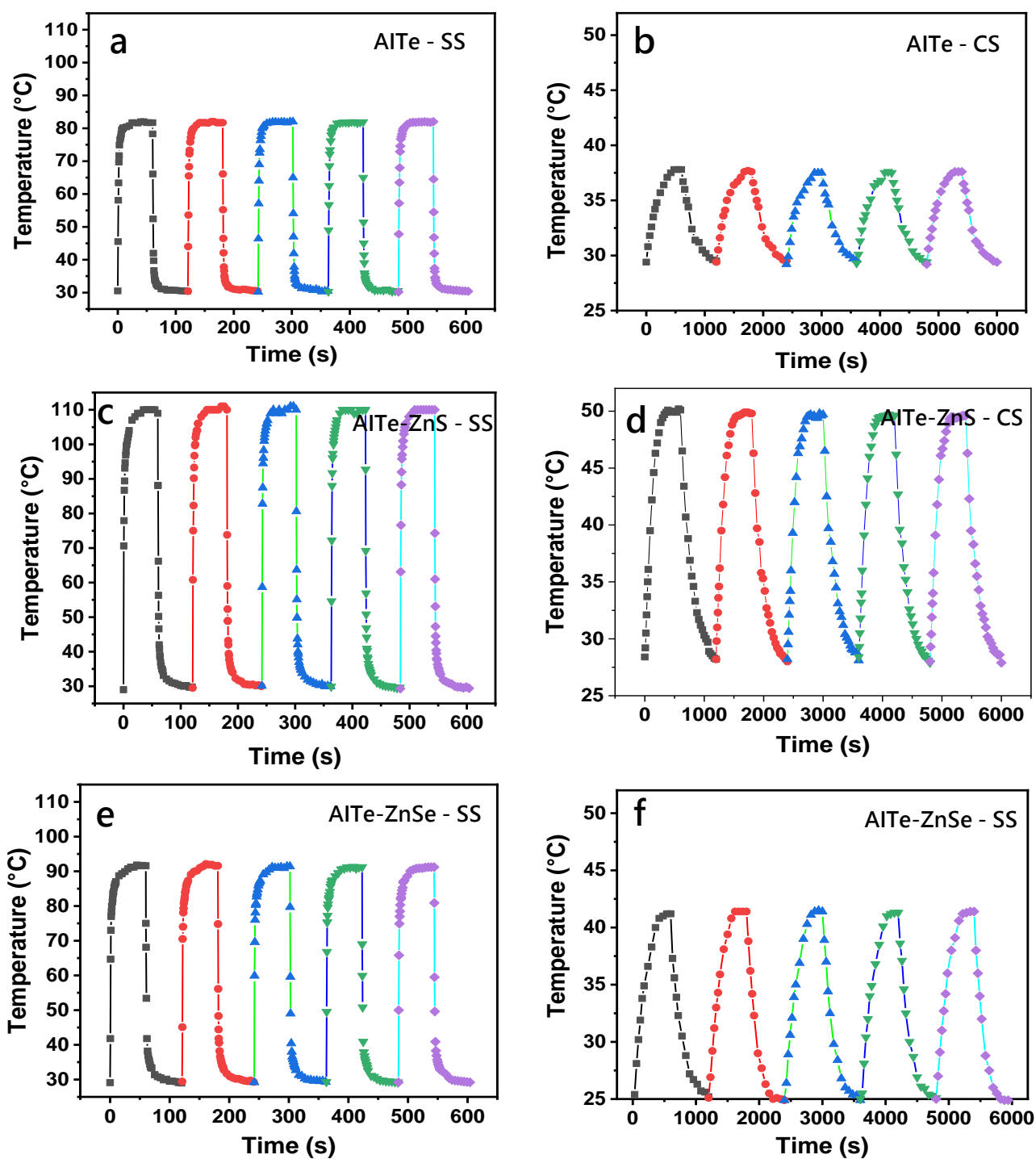
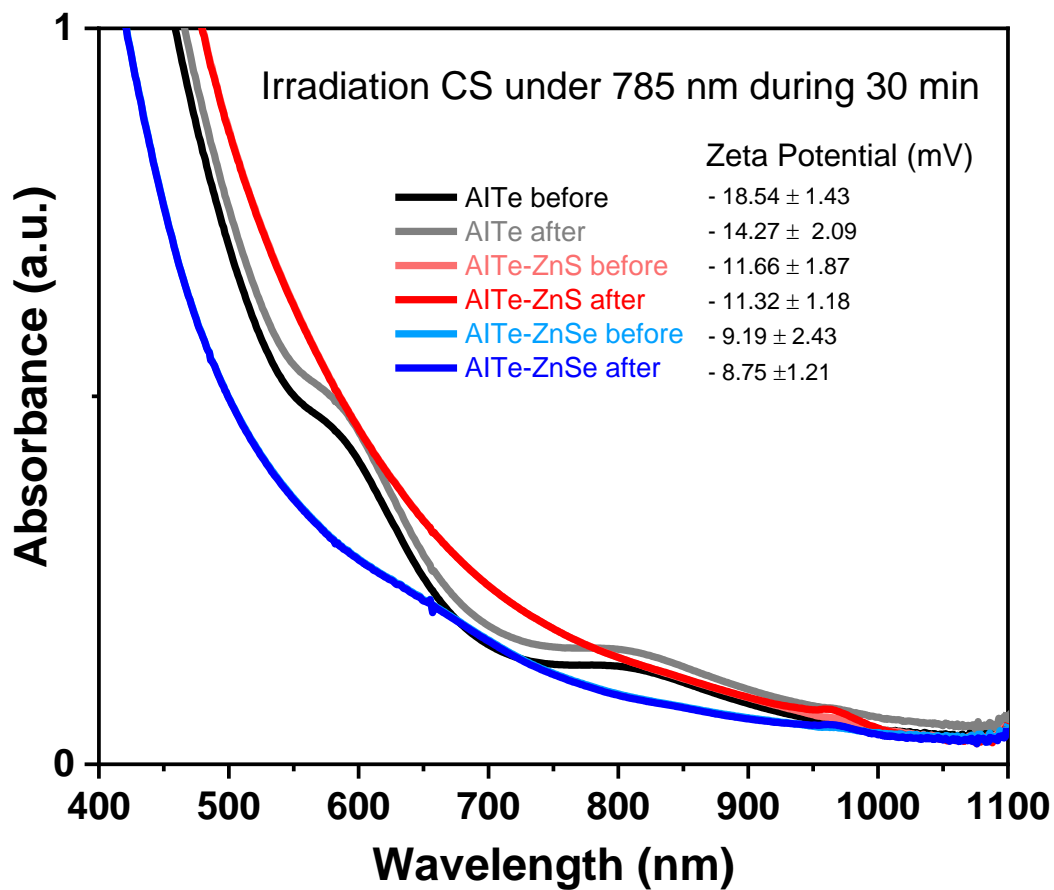


Figure S8. Influence of the laser power density (0.4, 0.6, 0.8 and 1.0 W.cm<sup>-2</sup>,  $\lambda_{exc} = 785$  nm) for (a) solid state (SS) and (b) colloidal solution (CS) of AITe NCs, (c) SS and (d) CS of AITe-ZnS NCs, and (e) SS and (f) CS of AITe-ZnSe NCs (M/Te<sup>2-</sup> ratio = 1:0.75; X<sup>2-</sup>/Te<sup>2-</sup> = 1:1).



**Figure S9.** Photothermal cycles for (a) solid state (SS) and (b) colloidal solution (CS) of AlTe NCs, (c) SS and (d) CS of AlTe-ZnS NCs, and (e) SS and (f) CS of AlTe-ZnSe NCs, under  $1.0 \text{ W.cm}^{-2}$  power density, and  $\lambda_{\text{exc}} = 785 \text{ nm}$ .



**Figure S10.** Absorption spectra and surface electrical charge of the AlTe, AlTe-ZnS, e AlTe-ZnSe colloidal solutions (CS), before and after 30 min of continuous irradiation at  $\lambda_{em} = 785$  nm and laser power =  $1.0 \text{ W.cm}^{-2}$ .

## 6. Photothermal conversion efficiency ( $\eta_T$ )

The linear time data *vs.*  $-\ln(\theta)$  obtained from the cooling period of Fig. S7 was represented for the nanocrystals synthesized (Fig. S9).

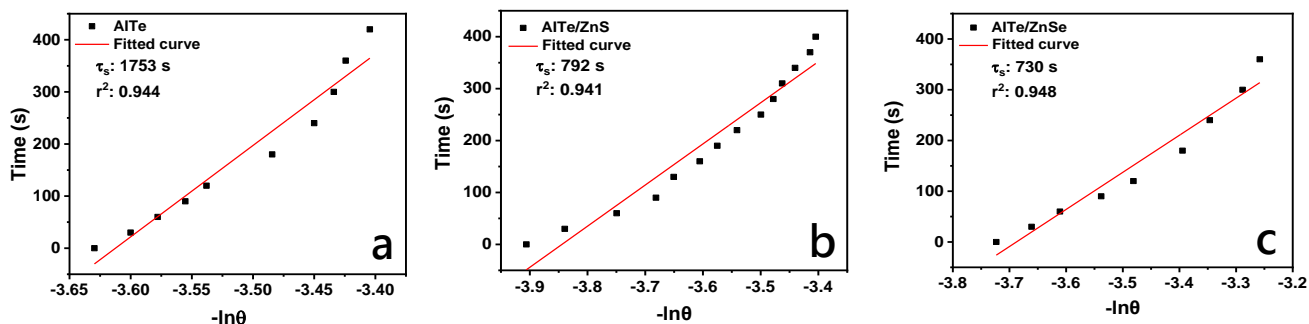


**Figure S11.** Adjustment of cooling curves as a function of time after irradiation (1.0  $\text{mW}\cdot\text{cm}^{-2}$ ) for (a) AlTe, (b) AlTe-ZnS, and (c) AlTe-ZnSe NCs.

The photothermal conversion efficiency to transform the absorbed radiation into heat can be calculated from equation 1.<sup>11</sup>

$$\eta_T = \frac{hA(T_{max} - T_{surr}) - Q_0}{I(1 - 10^{A_\lambda})} \quad (1)$$

where  $h$  is the heat transfer coefficient,  $A$  is the surface area of the container, and the  $hA$  value can be obtained from the linear fit of Figure S9.  $T_{max}$  is the maximum temperature reached and  $T_{surr}$  is the ambient temperature.  $I$  is the laser power (1 W) and  $A_\lambda$  is the absorbance (0.16) at the excitation wavelength of 785 nm.  $Q_0$  is relative to the absorption of radiation by the solution.

The  $\tau_s$  value can be obtained through equation 2:

$$hA = \frac{m_D C_D}{\tau_s} \quad (2)$$

where,  $\tau_s$  is the sample system time constant,  $m_D$  and  $C_D$  are the mass (1 g) and heat capacity ( $4.2 \text{ J}\cdot\text{g}^{-1}$ ) of water.  $Q_0$  was measured independently with deionized water,

presenting a value equal to 12.5 mW.°C. The calculated photothermal conversion efficiency of the systems was 14.9 %, 24.4 %, and 24.0 % for AlTe, AlTe/ZnS, and AlTe/ZnSe, respectively. The reported values are close to gold nanoparticles (21%), but below the performance of platinum nanoparticles (27.6%-52%) and PbS/CdS-RGD (48.3%).<sup>12-14</sup> Thus, it is possible to observe an improvement in the photoelectrochemical performance of semiconductors through structural modification and it allows to estimate its application for nanotheranostics, due to emission in the visible region.

## 7. Comparison among synthetic methodologies

A comparison among synthetic methods described in the literature was carried out, the data are described in Table S4. Synthetic and optical parameters were evaluated.

The synthesis in aqueous medium described in this work brings some advantages over reactions carried out in organic medium, Table S4. The four methods previously reported (Table S4, entries 1-6) show the use of reducing agents such as trioctylphosphine (TOPO) and lithium bis(trimethylsilyl)amide (LiN(SiMe<sub>3</sub>)<sub>2</sub>). In agreement to green chemistry, the electrochemical method described in this work allows atomic economy and avoids the use of harmful reducing agents. The reduction of the chalcogens occurs by direct electron transfer on the electrode surface, in a process controlled by electrical charge. The stabilizers proposed here, GSH and CA, are biocompatible, while the methods carried out in organic media use dodecanethiol as stabilizer, with low biocompatibility. In this work, the complete synthetic procedure involves a considerable shorter reaction time than those described in organic medium and mild reaction conditions. In addition, longer periods of heat treatment used in organic media are associated with different nucleation dynamics and growth of nanocrystals in low dielectric constant media (ODE dielectric constant = 2). However,

we can mention as a disadvantage of the electrochemical synthesis in aqueous medium, the difficulty to reach silver richer nanocrystals, which emission wavelength could shift to the NIR region. These silver richer AITe NCs can be synthesized in organic media, however, they were unstable in aqueous medium. The electrochemical method described in this work is an advance for the synthesis of AgIn<sub>5</sub>Te<sub>8</sub> NCs in water aiming biological applications, and it is the first description of the AITe photothermal properties.

**Table S4.** Experimental conditions of synthesis and properties of AITe NCs in recent literature.<sup>15-17</sup>

Entry	Nanocrystal	Strategy	Stabilizer	Te <sup>2-</sup> precursor/ synthesis conditions	Diameter (nm)	$\lambda_{em}$ (nm)	Ref.
1	AgInTe <sub>2</sub>	Hot injection/ODE <sup>a</sup>	DDT <sup>b</sup> /OLA <sup>c</sup>	Te <sup>0</sup> /TOPO <sup>f</sup> ; 170°C, 120 min	10.7	1101	[15]
2	AgInTe <sub>2</sub> @ZnS	Hot injection/ODE	DDT/OLA	Te <sup>0</sup> /TOPO; 170°C, 120 min	11	1005	[15]
3	AgInTe <sub>2</sub>	Hot injection/ODE	DDT	Te <sup>0</sup> /TOPO; LiN(SiMe <sub>3</sub> ) <sub>2</sub> <sup>g</sup> , 180-240°C, 180 min	9.5	900	[16]
4	AgInTe <sub>2</sub> @ZnSe	Hot injection/ODE	DDT	Te <sup>0</sup> /TOPO; LiN(SiMe <sub>3</sub> ) <sub>2</sub> , 180-240°C, 180 min	-	780	[16]
5	AgInTe <sub>2</sub>	Hot injection/ODE	DDT	Te <sup>0</sup> /TOPO; 180-240°C, 120 min	Rod-shaped	1040	[17]
6	AgInTe <sub>2</sub> @ZnTe	Hot injection/ODE	DDT	Te <sup>0</sup> /TOPO; 180-240°C, 120 min	Rod-shaped	897	[17]
7	AgIn <sub>5</sub> Te <sub>8</sub>	Electrossynthesis/H <sub>2</sub> O	GSH <sup>d</sup> /CA <sup>e</sup>	Te <sup>0</sup> /2e <sup>-</sup> ; 100 °C, 15 min	4.4	889	This work
8	AgIn <sub>5</sub> Te <sub>8</sub> -ZnS	Electrossynthesis/H <sub>2</sub> O	GSH/CA	Te <sup>0</sup> /2e <sup>-</sup> ; 100 °C, 15 min	5.2	685	This work
9	AgIn <sub>5</sub> Te <sub>8</sub> -ZnSe	Electrossynthesis/H <sub>2</sub> O	GSH/CA	Te <sup>0</sup> /2e <sup>-</sup> ; 100 °C, 15 min	5.3	625	This work

<sup>a</sup>ODE: octadecene; <sup>b</sup>DDT: dodecanethiol; <sup>c</sup>OLA: Oleylamine; <sup>d</sup>GSH: glutathione; <sup>e</sup>CA: citric acid; <sup>f</sup>TOPO: trioctylphosphine;

<sup>g</sup>LiN(SiMe<sub>3</sub>)<sub>2</sub>: Lithium bis(trimethylsilyl)amide.

## 8. References

- 1 D. V. Freitas, J. R. González-Moya, T. A. S. Soares, R. R. Silva, D. M. Oliveira, H. S. Mansur, G. Machado and M. Navarro, *ACS Appl. Energy Mater.*, 2018, **1**, 3636–3645.
- 2 S. G. B. Passos, D. V. Freitas, J. M. M. Dias, E. T. Neto and M. Navarro, *Electrochim. Acta*, 2016, **190**, 689–694.
- 3 R. R. Silva, D. V. Freitas, F. L. N. Sousa, A. C. Jesus, S. E. Silva, A. A. P. Mansur, S. M. Carvalho, D. S. Marques, I. C. Carvalho, W. M. Azevedo, H. S. Mansur and M. Navarro, *J. Alloys Compd.*, 2021, **853**, 156926.
- 4 A. M. Brouwer, *Pure Appl. Chem.*, 2011, **83**, 2213–2228.
- 5 P. Li, Q. Wang, G. Deng, X. Guo, W. Jiang, H. Liu, F. Li and N. T. K. Thanh, *Phys. Chem. Chem. Phys.*, 2017, **19**, 24742–24751.
- 6 S. S. Chetty, S. Praneetha, S. Basu, C. Sachidanandan and A. V. Murugan, *Sci. Rep.*, 2016, **6**, 26078.
- 7 M. Sandroni, R. Gueret, K. D. Wegner, P. Reiss, J. Fortage, D. Aldakov and M. N. Collomb, *Energy Environ. Sci.*, 2018, **11**, 1752–1761.
- 8 T. Chevallier, G. Le Blevenec and F. Chandezon, *Nanoscale*, 2016, **8**, 7612–7620.
- 9 S. Jeong, S. Yoon, S. Y. Chun, H. C. Yoon, N. S. Han, J. H. Oh, S. M. Park, Y. R. Do and J. K. Song, *J. Phys. Chem. C*, 2018, **122**, 10125–10132.
- 10 F. L. N. Sousa, D. V. Freitas, R. R. Silva, S. E. Silva, A. C. Jesus, H. S. Mansur, W. M. Azevedo and M. Navarro, *Mater. Today Chem.*, 2020, **16**, 100238.
- 11 B. Li, Q. Wang, R. Zou, X. Liu, K. Xu, W. Li and J. Hu, *Nanoscale*, 2014, **6**, 3274–3282.
- 12 B. Huang, J. Hu, H. Li, M.-Y. Luo, S. Chen, M. Zhang, Z.-J. Sun and R. Cui, *ACS Appl. Bio Mater.*, 2020, **3**, 1636–1645.
- 13 S. Tang, M. Chen and N. Zheng, *Small*, 2014, **10**, 3139–3144.
- 14 L. Cheng, C. Wang, L. Feng, K. Yang and Z. Liu, *Chem. Rev.*, 2014, **114**, 10869–10939.

- 15 M. A. Langevin, T. Pons, A. M. Ritcey and C. Nì. Allen, *Nanoscale Res. Lett.*, 2015, **10**, 1–4.
- 16 O. Yarema, M. Yarema, W. M. M. Lin and V. Wood, *Chem. Commun.*, 2016, **52**, 10878–10881.
- 17 T. Kameyama, Y. Ishigami, H. Yukawa, T. Shimada, Y. Baba, T. Ishikawa, S. Kuwabata and T. Torimoto, *Nanoscale*, 2016, **8**, 5435–5440.